Article

A molecular solution approach to synthesize electronic quality Cu2ZnSnS4 thin films

Wenbing Yang, Hsin-Sheng Duan, Kitty C. Cha, Chia-Jung Hsu, Wan-Ching Hsu, Huanping Zhou, Brion Bob, and Yang Yang

J. Am. Chem. Soc., **Just Accepted Manuscript** • DOI: 10.1021/ja312678c • Publication Date (Web): 13 Apr 2013

A molecular solution approach to synthesize electronic quality Cu_2ZnSnS_4 thin films

Wenbing Yang, Hsin-Sheng Duan, Kitty C. Cha, Chia-Jung Hsu, Wan-Ching Hsu, Huanping Zhou, Brion Bob, Yang Yang*

Department of Materials Science and Engineering, University of California Los Angeles, Los Angeles, CA 90095, USA

KEYWORDS: Molecular, Solution Processing, Thin Film, CZTS

ABSTRACT: Successful implementation of molecular solution processing from a homogeneous and stable precursor would provide an alternative, robust approach to process multinary compounds compared with physical vapor deposition. Targeting deposition of chemically clear, high quality crystalline films requires specific molecular structure design and solvent selection. Hydrazine (N2H4) serves as a unique and powerful medium, particularly to incorporate selected metallic elements and chalcogens into stable solution as metal chalcogenide complexes (MCC). However, not all the elements and compounds can be easily dissolved. In this manuscript, we demonstrate a paradigm to incorporate previously insoluble transitional metal elements into molecular solution as metal-atom hydrazine/hydrazine derivative complexes (MHHD), as exemplified by dissolving of the zinc constituent as Zn(NH2NHCOO)2(N2H4)2. Investigation into the evolution of molecular structure reveals the hidden roadmap to significantly enrich the variety of building blocks for soluble molecules design. The new category of molecular structures not only set up prototype to incorporate other elements of interests, also point the direction for other compatible solvent selection. As demonstrated from the molecular precursor combining Sn-/Cu-MCC and Zn-MHHD, ultra-thin film of CZTS was deposited. Characterization of transistor based on CZTS channel layer shows electronic properties comparable to CuInSe2, confirming the robustness of this molecular solution processing and the prospect of earth abundant CZTS for next generation photovoltaic materials. This paradigm outlines potentially a universal pathway, from individual molecular design using selected chelated ligands, and combination of building blocks in a simple and stable solution, to fundamentally change the way multinary compounds are processed.

Introduction

The earth abundant chalcogenides of copper, zinc and tin make up an important class of materials toward creating low cost and sustainable thin film solar cells, with the properties of direct band gap with large absorption coefficient.[1,2] A variety of deposition techniques that were rapidly developed in recent years, both vacuum based and non-vacuum solution process, had success in boosting the power conversion efficiency from 6% to 11.1%.[3–11] Though they are analogous to CIGS, several challenges still limit the full extension of photovoltaic properties for these materials to the levels of CIGS devices. They include the non-identified complex multinary phase diagram currently compromised with empirically established experience; and some identified materials issues, a narrow phase stability field, difficulty to control stoichiometry and phase purity.[2] In order to fully extend the potential for kesterite CZTS materials, of particular interest is to develop an effective processing platform to overcome the challenges associated with a multinary compound that contains volatile species.

Solution processing of kesterite materials draws great interest, not only because of the potential low cost, high throughput production, but also decent device performance due to the ease of control film composition and volatile phases. The use of metal salts (e.g. chlorides and nitrates) could be considered one of the easiest and the most intuitive ways to introduce the various constituent elements into a CZTS precursor solution, since these salts offer good solubility in water and alcohol.[12,13] The fabrication of monodisperse CZTS nanocrystals can lead to binary or ternary subcomponent nanoparticles, and enables a variety of synthetic approaches to control composition and phase formation by avoiding effects of the volatile precursor at high temperature.[67] Unfortunately, those approaches cannot avoid some unnecessary impurities in the form of long carbon-chain ligands that stabilize the NCs-based ink prerequisite to deposit uniform films in large areas. A new type of metal chalcogenide complex (MCC) usually prepared form hydrazine with excess chalcogen opens the door for a chemically clean NCs system without introducing unnecessary impurities.[14–16] Solutions based on all MCC-constituents do not have the suspension stability issue. Since the introduction of molecular solution approaches, high quality semiconducting films have been achieved: CIGS films deposited from the molecular level MCC precursor yields the highest efficiency for a pure solution deposition technique.[17,18] Unable to design a Zn-based MCC ligands, the hydrazine based slurry by making the compromise to use

particles of hydrazinium zinc chalcogenide and soluble MCC of Cu- and Sn-constituent, currently holds the most successful approach to fabricate kesterite CZTS photovoltaic devices.[4,5] However, the formation of the slurry tends to be finicky and the stability of the MCC-ligands and particle systems has not been addressed.

A fully dissolved molecular homogenous solution capable of yielding chemically clean films is the most simple and effective way to process films of a multinary compound system, with each elemental component independently adjustable to control composition and phase. However the limited solubility of materials terminated this MCC-concept only within the realm of few materials but not Zn/ZnS/ZnSe and other transition metal based chalcogenides of interest. Previously we reported a solution processed CZTS with fully dissolving zinc constituent using hydrazine derivatives (HD).[3] The introduction of the hydrazine derivative breaks the solubility limitation for previously insoluble materials. To fully understand the underlying mechanism in order to expand its application to other new materials systems, we investigated the evolution of Zinc-HD molecular structures in the dissolution process, solution stability and the phase evolution reacted with Cu-and Sn-constituent toward kesterite CZTS. The identification of MHHD molecular structure serves as a lighthouse for molecular design to potentially incorporate a variety of other interested elements forming a stable molecular solution, and compatible solvents exploration beyond hydrazine. Electronic properties based on CZTS transistors indicates the mobility is similar level as the analogue CIGS, which points toward a promising future for CZTS materials and device technology to reach the level of CIGS. The enrichment of individual or combined molecular solution components provides a simple complementary route to process multinary compound with the capability for robust composition control.

Results & Discussion

By introducing carbon dioxide into hydrazine, the zinc constituent was incorporated in hydrazine in a fully dissolved form coexisting with Sn-S solution. **Figure 1A** shows the Zn/Sn precursor solution containing Zn- and Sn-constituent with the flexibility to adjust the metallic ratio. To achieve the soluble colorless solution, first, elemental zinc constituent was combined with hydrazinocarboxylic (hyc) acid in hydrazine with bubbling observed when combining the reactants. Unlike the dimension reduction of metal chalcogenide framework for the dissolution of soluble metal chalcogenides (SnS_2, In_2Se_3, Cu_2S) into hydrazine solution,[19] the metallic zinc lattice was dismantled and coordinated with chelate NH_2NHCOO through the reaction(1) .

$$Zn + NH_2NHCOOH \rightarrow [Zn(NH_2NHCOO)_3]^- + H_2(g) \quad (1)$$

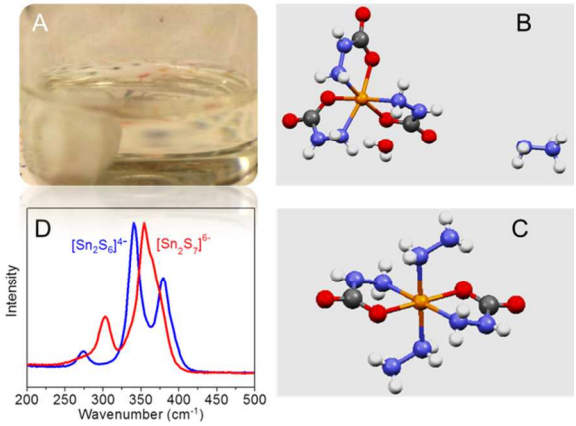

Figure 1. (A) Zn/Sn solution in hydrazine, by combining zinc precursor reacted from metallic zinc and hydrazidocarboxylic acid, SnS_2 solution precursor in hydrazine and extra sulfur. Atomic ratio between Zn and Sn is independently adjustable by controlling zinc precursor and Sn-solution. (B) crystal structure of $N_2H_5[Zn(NH_2NHCOO)_3]\cdot H_2O$ derived from the reaction of Zn and $NH_2NHCOOH$ in water. (C) crystal structure of $Zn(NH_2NHCOO)_2(N_2H_4)_2$, the soluble zinc complex from Zn/Sn solution in Figure 1A. (D) Solutoin Raman spectroscopy of Sn-S species in SnS_2 solution and Zn/Sn solution in Figure 1A.

To investigate the resulting molecular structure, a crystal was grown from the Zn and NH2NHCOOH species in an H2O based solution by slowly evaporating the solvent until the concentration saturated and precipitation began. **Figure 1B** shows the molecular structure of $Zn(hyc)_3$ resolved from X-ray crystallography. Zinc atom was chelated by three hyc bidentate ligands with Zn-N and Zn-O bond, the complex ion was electronically neutralized by hydrazinium cation $N_2H_5^+$, and the solvent molecular does not chemically bonded to zinc atom but as a neutral spacer between ions. Rather than using extra chalcogen to dissolve soluble metal chalcogenide into hydrazine, in which excess sulfur inserted between metal-chalcogenide covalent bond terminates the metal-chalcogenide framework, here it is the chelates ligands that dismantle metallic zinc lattice to form the individual unit of Zn-hyc complex. But the complex in **Figure 1B** still has a limited solubility in hydrazine existing as a white paste after continuous stirring. It was discovered that adding Sn-constituent (1 mmol) with excess sulfur (0.5 mmol) into the zinc paste (1 mmol) greatly improves the solubility, forming the mixed Zn/Sn precursor with a [Zn/Sn] concentration around 1M in this study.

$$[Zn(NH_2NHCOO)_3]^- + [Sn_2S_6]^{4-} + S + N_2H_4 \rightarrow Zn[NH_2NHCOO]_2[N_2H_4]_2 + [Sn_2S_7]^{6-} \quad (2)$$

To ascertain the molecular structure evolution, x-ray crystallography was applied to analyze the crystal of Zn-compound grown from Zn/Sn solution to by introducing H_2O as precipitant very carefully as shown in Figure **1C.** Zinc atom is chelated by two $NH_2NHCOOH$ and NH_2NH_2 molecules. The incorporation of hydrazine into the zinc complex forms $Zn(NH_2NHCOO)_2(N_2H_4)_2$ which exhibits greatly improved solubility compared with $Zn(hyc)_3$.The Sn-complex evolution from Sn_2S_6 to a S-rich complex during the reaction was revealed by Ra-

man spectroscopy on the molecular species in solution, as shown in **figure 1D**. Before mixing with the Zn-constituent, the Sn-solution with the molecular structure of $[Sn_2S_6]^{4-}$ shows the bridging mode (Sn-S-Sn) and stretching mode at 344 $cm^{-1}$and 367 cm^{-1} respectively, and the Sn_2S_2 ring vibration mode at 280 cm^{-1}.[20] While in the mixed Zn/Sn solution, the disappearance of Sn_2S_2 ring vibration mode at 280 cm^{-1} and the appearance of peaks around 300 cm^{-1} and 351 cm^{-1} suggest that excess sulfur terminates the symmetric Sn-S-Sn bridges in Sn_2S_6 to generate new bridge vibration in $S_3Sn–S–SnS_3$ and SnS_4 stretching mode around 348 cm^{-1}.[21,22] Gradually increasing the amount of sulfur in Zn/Sn solution leads to relatively stronger signal around 350 cm^{-1}, showing relatively larger portion of the SnS_4 species in a Sn-S complex.[22] Thus, the Zn/Sn solution in **Figure 1A** has the soluble form of $Zn(hyc)_2(N_2H_4)_2$ coexisting with multiple Sn-S species in equilibrium, including $[Sn_2S_7]$ and $[SnS_4]$, determined by the amount of extra sulfur incorporated. The zinc constituent is effectively incorporated into N_2H_4 solution with greatly enhanced solubility coexisting with Sn-S complex through chelation by two hydrazine molecules. This model, demonstrated in the case of zinc, to form both HD and N_2H_4 chelated complexes, is expected to provide a universal route to possibly incorporate previously non-soluble elements into hydrazine and other solvents.

As-prepared colorless Zn/Sn solution is stable for several months in an inert atmosphere. Even in the process of evaporating hydrazine solvent, no obvious precipitates showed up until the eventual transparent amorphous solid with a slight yellowish color. The zinc compound remained until the chemical environment was changed by introducing S-ligands. It was observed that adding extra sulfur into the Zn/Sn solution (Figure 1A) with S-H ligands generates precipitates within several days. While in a stable Zn/Sn solution, no obvious S-H signal at 2560 cm^{-1} was observed via Raman spectroscopy. As shown in ***Figure* 2A**, the introduction of 1 mmol excess S into 1 ml Zn/Sn solution forms $(N_2H_5)HS$ or $((N_2H_5)_2S$, which is evident by a strong Raman S-H signal.[23] The appearance of S-ligands in the system varies the complex coordination on the zinc atom: the formation of thermodynamically favorable Zn-S bond tends to strip the coordinated ligands of hyc and hydrazine molecular by replacing the Zn-N, Zn-O bond.

$$Zn[NH_2NHCOO]_2[N_2H_4]_2 + SH[N_2H_5] \rightarrow ZnS + N_2H_4 + NH_2NHCOOH \quad (3)$$

Composition analysis by XPS (Figure 2B) showed that the S-ligands destroy the stability of zinc complex solution system, forming a ZnS precipitation within 1 day at room temperature. As it is thermodynamically stable, ZnS precipitated from the solution containing S-ligands. This behavior is consistent with the mostly insoluble nature of ZnS using the approach of introducing excess sulfur into hydrazine.[17]

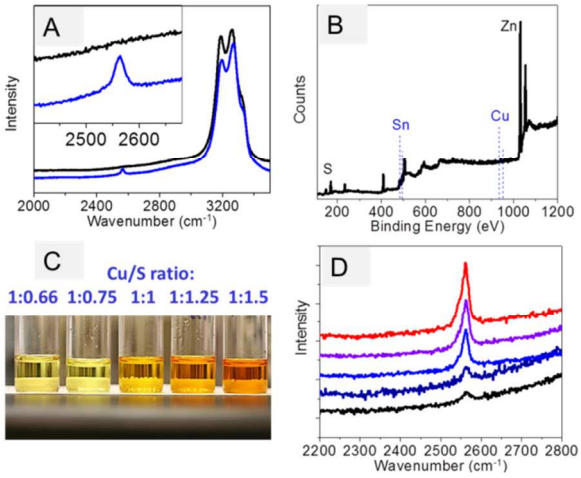

Figure 2. Stability of molecular species. (A) Raman spectrosopy from Zn/Sn solution in figure 1A. Incorporating extra sulfur leads to the formation of S-ligands with Raman signal at 2560 cm^{-1}. (B) XPS result of precipitation formed adding excess S into Zn/Sn solution. (C) Cu-precursors with a serial of Cu:S ratio from 1:1.5 to 1:0.75. (D) Raman spectroscopy on Cu-precursors showing the normalized intensity of S-ligands in solution.

The effect of S-ligands on the stability of final CZTS precursor has also been verified when mixing with a serial of Cu-S-N_2H_4 solutions with decreasing S/Cu ratio. **Figure 2C** shows the freshly made Cu-constituent solutions: the color shift from yellow to brown is attributed to the absorption from increasing the excess sulfur dissolved in hydrazine solution. The normalized S-H vibration signal from the solution-phase Raman spectrum at 2560 cm^{-1} (**Figure 2D**) reveals reduced S-ligands with lower excess S. When mixing the Zn/Sn solution with a S-rich Cu-constituent (S:Cu~1.5), obvious precipitation of ZnS was observed after several hours. The composition analysis by XPS on the precipitates shows strong Zn and S signal while the absence of Sn- and Cu-signal (Figure 2B). The mixed solution of the Cu-constituent with a smaller S ratio is stable for several days. The final mixture of a Zn/Sn solution with a Cu-constituent of S/Cu~0.75, with a barely visible S-H signal in Raman spectroscopy, was stable for several weeks without obvious aggregation. It is indicated that Zn-complex could also coexist with Cu-constituent as the form of $Cu_6S_4^{4-}$. The stability collapse in the mixed CZTS precursor behaves similarly to that of the Zn/Sn solution with extra sulfur. Therefore, by extrapolation of these findings, to achieve stable multinary molecular solutions, the incorporation of S-ligands should be avoided when combining Zn- or other metallic complex with hydrazine/hydrazine derivative chelates of other constituents

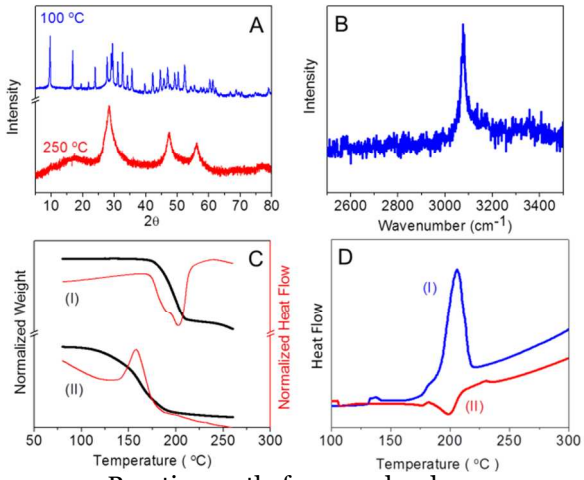

Figure 3. Reaction path from molecular precursor to kesterite CZTS phase. (A) X-ray diffraction patterns (B) Raman spectrum for CZTS precursors annealed with the maximum temperature at 100 °C and 250 °C. (C) Thermogravimetric analysis (TGA) on (I) $Zn(hyc)_3$, showing endothermic reaction around 200 °C, and (II)CZTS precursor toward kesterite phase with an exothermic decomposition around 150 °C. (D) Differential scanning calorimetry analysis on $Zn(hyc)_3$ and CZTS precursor.

The molecular solution process provides a platform to further examine the mechanism of transformation from precursor solutions to a solid film with the desired phase. Compared with the solid state reaction routes that coverts binary phases into CZTS as demonstrated in hydrazine slurry precursor and thermal evaporation,[5,7,24] the molecular solution yields final phase from individual molecular in a single step. The final CZTS precursor solution has the flexibility to realize compositional control by varying the volume of each constituent solution. The evolution of the zinc complex with hydrazine incorporated as chelate ligands, shrinks the thermal barrier to release Zn. Compared with $Zn(hyc)_3$ complex, which decomposed into metal/metal oxide powder above 500°C with the major endothermic reaction around 200°C; in contrast, the CZTS precursor containing hydrazine coordinated Zn-complex shows exothermic behavior around 160°C as shown in **Figure 3C**. The exothermic process is partially due to the incorporation of the hydrazine molecule on a zinc atom and hydrazinium species from Cu- and Sn-components.[15] Another possible route is likely from the chemical modification of the Zn complex by sulfur ligands. While extra S-ligands tend to disturb the stability of the solution system, control of the S-ligands during film processing also provides a self-cleaning procedure to chemically strip hyc ligands from zinc. The differential scanning calorimetry analysis on $Zn(hyc)_3$ and CZTS precursor (**Figure 3D)** also shows the opposite thermal behavior, suggesting molecular structure evolution had occurred in zinc complex system. Therefore, rather than solely thermal decomposition of the Zn-complex, S-ligands also provide an extra chemical route to extract zinc by replacing the coordinate ligands, which is accelerated by intermediate annealing. As a result, on a molecular scale, the homogeneously released zinc constituent reacts with Sn- and Cu-MCC molecular species, contributing to the kinetically favorable reaction path to form CZTS phase at a low temperature around 200°C without involving any long-range diffusion process.

$$[Cu_6S_4]^{2-} + Zn[NH_2NHCOO]_2[N_2H_4]_2 + [Sn_2S_6]^{4-} + S + N_2H_5^+ \xrightarrow{T} \text{CZTS + volatile species } (N_2H_4, CO_2) \quad (4)$$

The stripped molecule $NH_2NHCOOH$ itself evolved to gaseous species around 160°C, much lower than the decomposition of coordinated form. Further annealing up to 250°C leads to the dissociation of hydrazine/ hydrazium/ hydrazine derivative into volatile species (CO_2 and hydrazine).[25] Phase characterization of the product by XRD further verifies the evolution process regarding the dissociation of the spacer molecule. The strong diffraction peak at 8° in **Figure 3A** from the powder derived from evaporating solvent of CZTS precursor, indicates a large d-spacing possibly separated by $N_2H_5^+$/ N_2H_4, which agrees well with other hydrazium compounds.[26] The N-H stretching signal from the Raman spectrum (**Figure 3B**) also suggests the existence of $N_2H_5^+$/ N_2H_4 spacer. The disappearance of the N-H signal upon the intermediate heat treatment of 250°C is coherent with the simple thermal decomposition step from the hydrazium complex system to the metal chalcogenide product. For wider applications, the molecular solution process, with the capability to acquire single phase, chemically clean films, also provides a platform to examine the material properties correlating its structure and electrical performance.

The crystalline semiconducting films were spin coated from CZTS molecular precursor solution, which allows the deposition of a continuous smooth film thinner than 10 nm. From atomic force microscope (AFM) in **Figure 4A**, the roughness of the film is within the range of 2nm. The volatile nature of hydrazinium cation and hydrazine derivative enables the formation of chemically clean highly crystalline CZTS phase below 250°C. Upon 400 °C annealing, the chemical composition analysis (**Figure 4B**) on films by RBS indicates negligible carbon impurity left in the resulting films. A highly crystalline kesterite CZTS phase is obtained without any non-identified phases as indicated in XRD (**Figure S1**). The demonstrated film uniformity realized from all the components of CZTS phase on the molecular level, enables the deployment of potential scaled-up deposition of large area films on both rigid and flexible substrates at relatively low temperature.

TFTs using ultra-thin channel layer of CZTS films deposited this way have been demonstrated in the architecture shown in **figure 4C,** using thermally evaporated gold as source and drain electrodes. The representative output of drain current vs drain voltage as a function of applied gate voltage is plotted in **Figure 4D** with a CZTS channel layer. The device functioned as a p-channel transistor, operating at accumulation mode under the field provided by a negative applied gate voltage, while positive gate voltage depletes the channel layer and turns the device off. The current-voltage curve shows typical transistor behavior with a linear I_d/V_d dependence ini-

tially and saturated as channel layer was pinched off. A typical transfer curve with the relation of gate bias V_g dependent drain current I_d was shown in **Figure 4F**, indicating an on/off ratio of 10^2. The relatively low on/off ratio is related to the kesterite CZTS phase which exists only in a very narrow stoichiometric window and small deviations of composition usually generates detrimental secondary phases.[27] Previously reported mobility and carrier density located in the high range of carrier density ($10^{18}/cm^3$) and mobility (beyond 10 $cm^2/(V \cdot s)$) may be partially due to the contribution of resulting impurity phases.[2] To exclude possible non-shut off current contributed from impurity conductive phase in the channel layer, the saturation region mobility is calculated from the linear relation of I_d vs V_g, yielding the value of 1.3$cm^2/(V \cdot s)$. The mobility of CZTS is comparable with CISS materials demonstrated from the transistor device using similar hydrazine deposition.[28]

$$I_D = \frac{\mu}{2} C_{ox} \frac{W}{L} \left(V_g - V_{th}\right)^2 \quad (5)$$

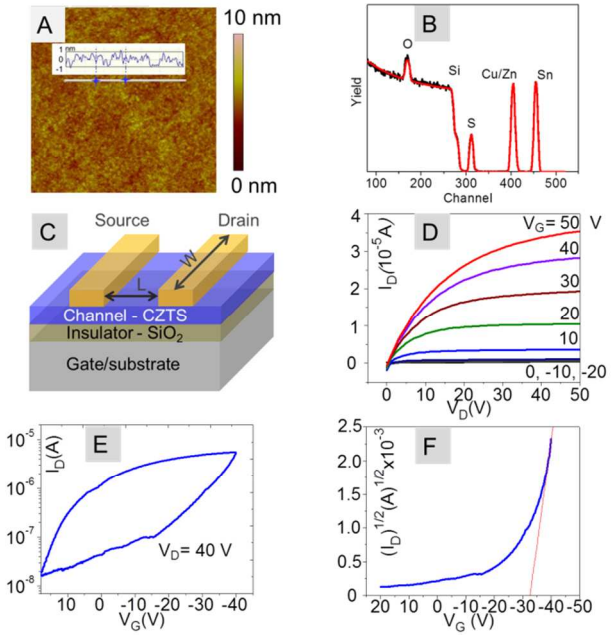

Figure 4. (A) Atomic Force Microscopy (AFM) shows the roughness of less than 2 nm for CZTS films deposited on Si/SiO_2 substrate subjected thermal treatment under 400 °C. (B) composition analysis on CZTS film by Rutherford Back Scattering (RBS). The possible impurity of carbon is under the detection limitation of RBS. (C)schematic of transistor structure using CZTS film as channel layer (channel length L = 200 μm, channel width W = 5000 μm), gold as source and drain electrode on SiO_2/Si substrates using heavily doped Si as gate terminal. (D) a typical source drain output of CZTS transistor plotted of I_{sd} (drain current) as a function V_{sd} (drain voltage) when applying different V_g (gate voltage) (E) hysteris effect of CZTS channel layer based transistor. (F) gate voltage dependent drain current at saturation region.

The hysteresis effect shown in **Figure 4E**, normally found in polycrystalline thin films but extremely obvious in the CZTS system, suggest a large number of hole traps at grain boundaries and interfaces between the channel layer and substrate or electrode. Future work to passivate electrically active defects at the grain boundary or interface, such as introducing potential elements from the convenient precursor solution processing platform, is expected to further advance the property of CZTS material system. The defects engineering to minimize the hysteresis effect and optimize CZTS transistor behavior would also be critical to inspire the breakthrough on its photovoltaic performance comparable with analogue CIGS materials system.

Conclusion

The discovery and design on new category of molecular structure, empowers molecular solution process a simple and potentially universal way to process complex multinary compounds. As demonstrated in CZTS complex system, ultrathin kesterite film of high quality crystallinity is reported using hydrazine/hydrazine derivative as chelate ligands to incorporate zinc homogeneously with Cu-and Sn-constituents of MCC molecules. By introducing volatile ligands chelating on elemental metals of interest, an extended realm of materials can be unprecedentedly pocessed by the simple molecular solution process. This method is capable of controlling the composition precisely and resulting phase purity, generating homogenous, chemically clean films, comparable with other PVD approaches. Transistors using the resulting CZTS channel layer indicated a comparable mobility value with the analogue CIGS materials, which points out the strong potential for kesterite CZTS to achieve higher performance for PV devices. The molecular solution process using chelate ligands provides a general platform to incorporate other transition metals into a molecular processor, especially in the way of composition control and phase uniformity, to yield high performance semiconducting films for optoelectronics applications.

ASSOCIATED CONTENT

Supporting Information. Experiment data on solution preparation, device fabrication, materials characterization. This information is available free of charge via the Internet at http://pubs.acs.org/.

AUTHOR INFORMATION

Corresponding Author

* E-mail address: yangy@ucla.edu (Y. Yang).
Tel.: +1 310 825 4052; Fax: +1310 825 3665.

ACKNOWLEDGMENT

The authors would like to acknowledge Dr Saeed Khan for analyzing crystal structure of Zn-complexes using single-crystal X-ray diffraction. Valuable technical discussion with Mr. Min Xue and Mr. Eric Richard is also appreciated.

REFERENCES

(1) Katagiri, H.; Jimbo, K.; Maw, W. S.; Oishi, K.; Yamazaki, M.; Araki, H.; Takeuchi, A. *Thin Solid Films* **2009**, *517*, 2455–2460.

(2) Mitzi, D. B.; Gunawan, O.; Todorov, T. K.; Wang, K.; Guha, S. *Solar Energy Materials and Solar Cells* **2011**, *95*, 1421–1436.

(3) Yang, W.; Duan, H.-S.; Bob, B.; Zhou, H.; Lei, B.; Chung, C.-H.; Li, S.-H.; Hou, W. W.; Yang, Y. *Advanced materials (Deerfield Beach, Fla.)* **2012**, *24*, 6323–6329.

(4) Todorov, T. K.; Tang, J.; Bag, S.; Gunawan, O.; Gokmen, T.; Zhu, Y.; Mitzi, D. B. *Advanced Energy Materials* **2012**, *3*, 34–38.

(5) Todorov, T. K.; Reuter, K. B.; Mitzi, D. B. *Advanced materials (Deerfield Beach, Fla.)* **2010**, *22*, E156–9.

(6) Guo, Q.; Ford, G. M.; Yang, W.-C.; Walker, B. C.; Stach, E. a; Hillhouse, H. W.; Agrawal, R. *Journal of the American Chemical Society* **2010**, 17384–17386.

(7) Cao, Y.; Denny, M. S.; Caspar, J. V; Farneth, W. E.; Guo, Q.; Ionkin, A. S.; Johnson, L. K.; Lu, M.; Malajovich, I.; Radu, D.; Rosenfeld, H. D.; Choudhury, K. R.; Wu, W. *Journal of the American Chemical Society* **2012**, *134*, 15644–7.

(8) Shin, B.; Gunawan, O.; Zhu, Y.; Bojarczuk, N. A.; Chey, S. J.; Guha, S. *Progress in Photovoltaics: Research and Applications* **2013**, *21*, 72–76.

(9) Repins, I.; Beall, C.; Vora, N.; DeHart, C.; Kuciauskas, D.; Dippo, P.; To, B.; Mann, J.; Hsu, W.-C.; Goodrich, A.; Noufi, R. *Solar Energy Materials and Solar Cells* **2012**, *101*, 154–159.

(10) Chawla, V.; Clemens, B. In *2012 38th IEEE Photovoltaic Specialists Conference*; IEEE, 2012; pp. 002990–002992.

(11) Sugimoto, H.; Hiroi, H.; Sakai, N.; Muraoka, S.; Katou, T. In *2012 38th IEEE Photovoltaic Specialists Conference*; IEEE, 2012; pp. 002997–003000.

(12) Hibberd, C. J.; Chassaing, E.; Liu, W.; Mitzi, D. B.; Lincot, D.; Tiwari, a. N. *Progress in Photovoltaics: Research and Applications* **2010**, *18*, 434–452.

(13) Ki, W.; Hillhouse, H. W. *Advanced Energy Materials* **2011**, *1*, 732–735.

(14) Kovalenko, M. V; Scheele, M.; Talapin, D. V *Science (New York, N.Y.)* **2009**, *324*, 1417–20.

(15) Mitzi, D. B.; Kosbar, L. L.; Murray, C. E.; Copel, M.; Afzali, A. *Nature* **2004**, *428*, 299–303.

(16) Jiang, C.; Lee, J.-S.; Talapin, D. V *Journal of the American Chemical Society* **2012**, *134*, 5010–3.

(17) Mitzi, D. B.; Todorov, T. K.; Gunawan, O.; Yuan, M.; Cao, Q.; Liu, W.; Reuter, K. B.; Kuwahara, M.; Misumi, K.; Kellock, A. J.; Chey, S. J.; De Monsabert, T. G.; Prabhakar, A.; Deline, V.; Fogel, K. E. In *2010 35th IEEE Photovoltaic Specialists Conference*; IEEE, 2010; pp. 000640–000645.

(18) Todorov, T. K.; Gunawan, O.; Gokmen, T.; Mitzi, D. B. *Progress in Photovoltaics: Research and Applications* **2012**, *21*, 82–87.

(19) Mitzi, D. B. *Advanced Materials* **2009**, *21*, 3141–3158.

(20) Pienack, N.; Lehmann, S.; Lühmann, H.; El-Madani, M.; Näther, C.; Bensch, W. *Zeitschrift für anorganische und allgemeine Chemie* **2008**, *634*, 2323–2329.

(21) Nasn, D. S. Von; Schlwy, W. *Z. anorg. allg. chem.* **1973**, *398*, 63–71.

(22) Campbell, J.; DiCiommo, D. P.; Mercier, H. P. A.; Pirani, A. M.; Schrobilgen, G. J.; Willuhn, M. *Inorganic Chemistry* **1995**, *34*, 6265–6272.

(23) Chung, C.-H.; Li, S.-H.; Lei, B.; Yang, W.; Hou, W. W.; Bob, B.; Yang, Y. *Chemistry of Materials* **2011**, *23*, 964–969.

(24) Hsu, W.-C.; Repins, I.; Beall, C.; DeHart, C.; To, B.; Yang, W.; Yang, Y.; Noufi, R. *Progress in Photovoltaics: Research and Applications* **2012**, DOI: 10.1002/pip.2296.

(25) Yuan, M.; Mitzi, D. B. *Dalton transactions (Cambridge, England□: 2003)* **2009**, 6078–88.

(26) Hsu, W.-C.; Bob, B.; Yang, W.; Chung, C.-H.; Yang, Y. *Energy & Environmental Science* **2012**, *5*, 8564.

(27) Chen, S.; Yang, J.-H.; Gong, X. G.; Walsh, A.; Wei, S.-H. *Physical Review B* **2010**, *81*, 245204–.

(28) Milliron, D. J.; Mitzi, D. B.; Copel, M.; Murray, C. E. *Chemistry of Materials* **2006**, *18*, 587–590.

Table of Content:

Title: A molecular solution approach to synthesize electronic quality Cu_2ZnSnS_4 thin films

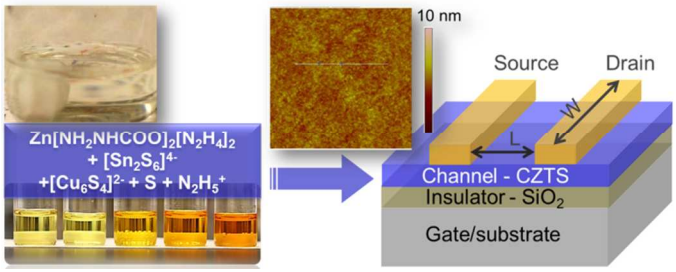

Figures

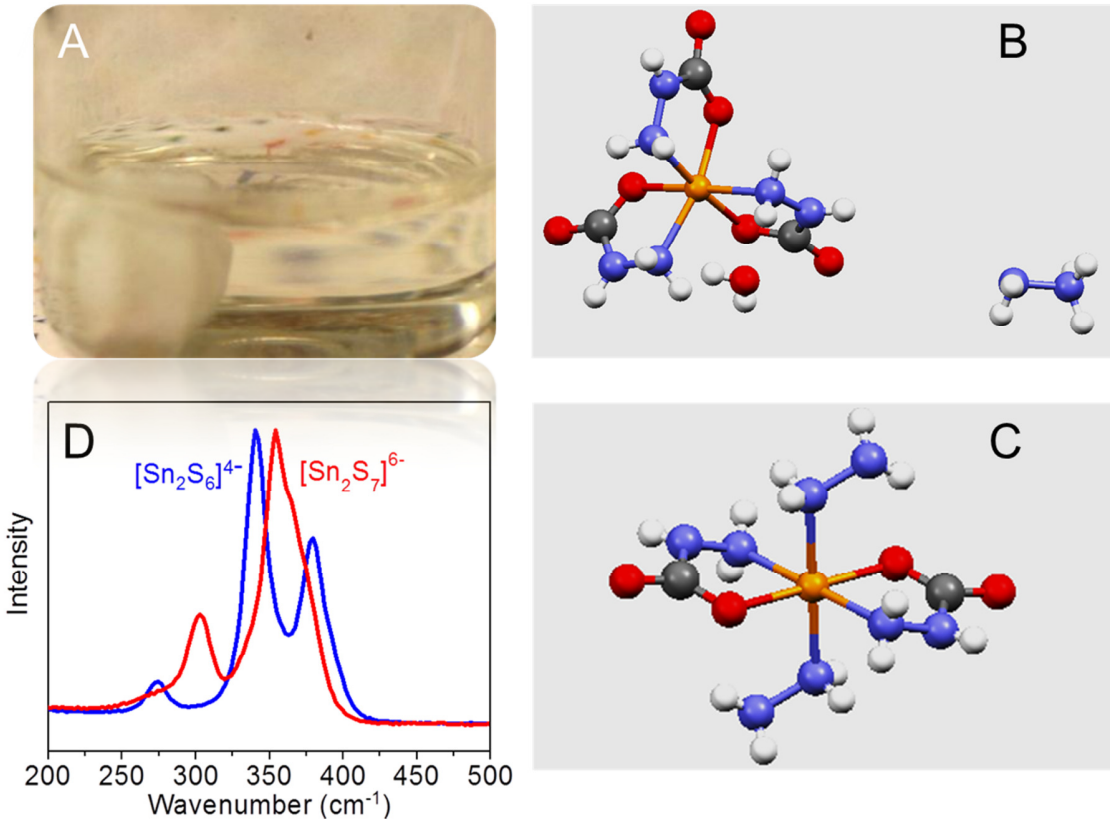

Figure 1 (A) Zn/Sn solution in hydrazine, by combining zinc precursor reacted from metallic zinc and hydrazidocarboxylic acid, SnS_2 solution precursor in hydrazine and extra sulfur. Atomic ratio between Zn and Sn is independently adjustable by controlling zinc precursor and Sn-solution. (B) crystal structure of $N_2H_5[Zn(NH_2NHCOO)_3]\cdot H_2O$ derived from the reaction of Zn and $NH_2NHCOOH$ in water. (C) crystal structure of $Zn(NH_2NHCOO)_2(N_2H_4)_2$, the soluble zinc complex from Zn/Sn solution in Figure 1A. (D) Solutoin Raman spectroscopy of Sn-S species in SnS_2 solution and Zn/Sn solution in Figure 1A.

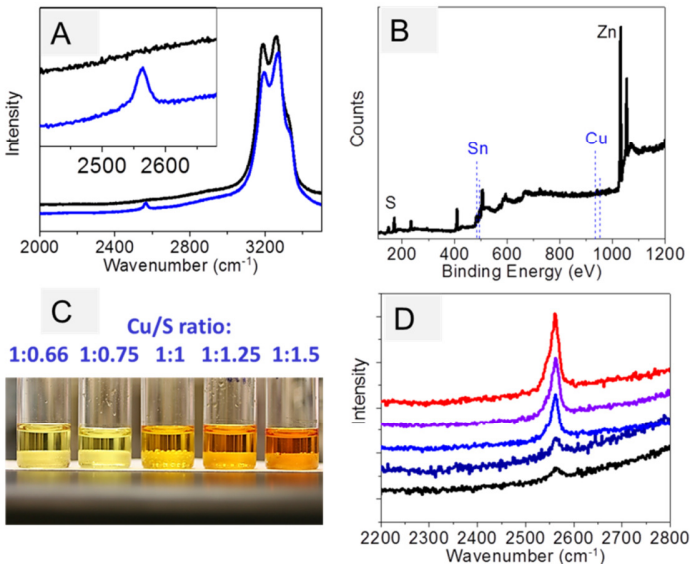

Figure 2. Stability of molecular species. (A) Raman spectrosopy from Zn/Sn solution in figure 1A. Incorporating extra sulfur leads to the formation of S-ligands with Raman signal at 2560 cm^{-1}. (B) XPS result of precipitation formed adding excess S into Zn/Sn solution. (C) Cu-precursors with a serial of Cu:S ratio from 1:1.5 to 1:0.75. (D) Raman spectroscopy on Cu-precursors showing the normalized intensity of S-ligands in solution.

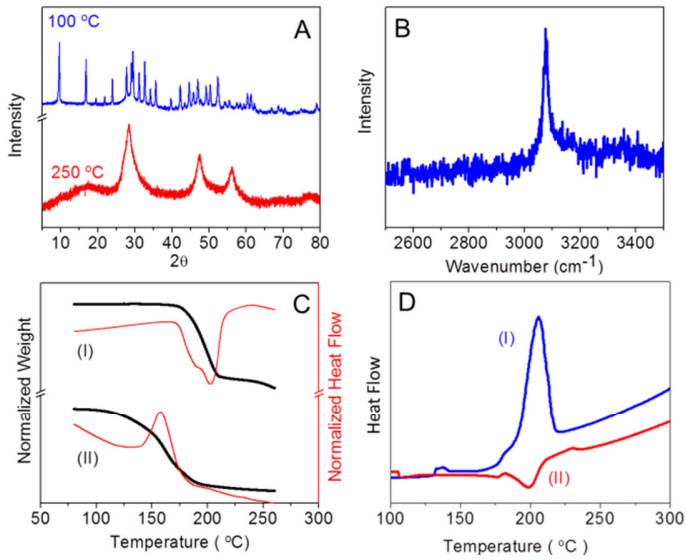

Figure 3. Reaction path from molecular precursor to kesterite CZTS phase. (A) X-ray diffraction patterns (B) Raman spectrum for CZTS precursors annealed with the maximum temperature at 100 ^{o}C and 250 ^{o}C. (C) Thermogravimetric analysis (TGA) on (I) $Zn(hyc)_3$, showing endothermic reaction around 200 ^{o}C, and (II)CZTS precursor toward kesterite phase with an exothermic decomposition around 150 ^{o}C. (D) Differential scanning calorimetry analysis on $Zn(hyc)_3$ and CZTS precursor.

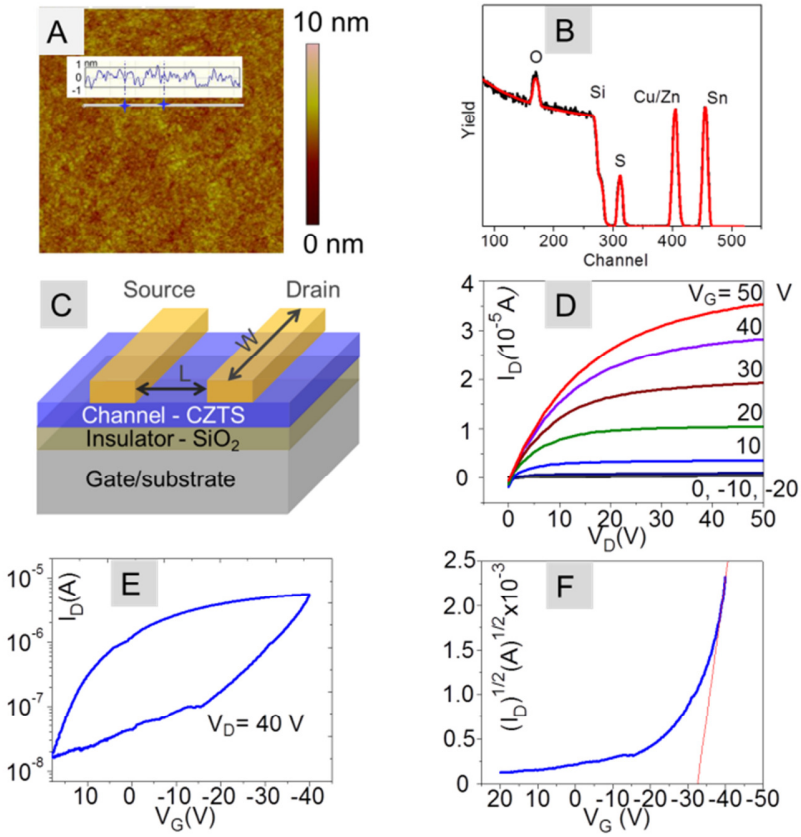

Figure 4. (A) Atomic Force Microscopy (AFM) shows the roughness of less than 2 nm for CZTS films deposited on Si/SiO_2 substrate subjected thermal treatment under 400 ^{o}C. (B) composition analysis on CZTS film by Rutherford Back Scattering (RBS). The possible impurity of carbon is under the detection limitation of RBS. (C)schematic of transistor structure using CZTS film as channel layer (channel length L = 200 μm, channel width W = 5000 μm), gold as source and drain electrode on SiO_2/Si substrates using heavily doped Si as gate terminal. (D) a typical source drain output of CZTS transistor plotted of I_{sd} (drain current) as a function V_{sd} (drain voltage) when applying different V_g (gate voltage) (E) hysteris effect of CZTS channel layer based transistor. (F) gate voltage dependent drain current at saturation region.